

**Supplementary Materials for:**  
**Time-dependent Shear Rate Inhomogeneities and Shear Bands in**  
**a Thixotropic Yield-Stress Fluid under Transient Shear**

Yufei Wei, Michael J. Solomon, and Ronald G. Larson<sup>a)</sup>

*Department of Chemical Engineering, University of Michigan,*

*Ann Arbor, Michigan, 48105*

**1. Schematic of the rheo-PIV instrument**

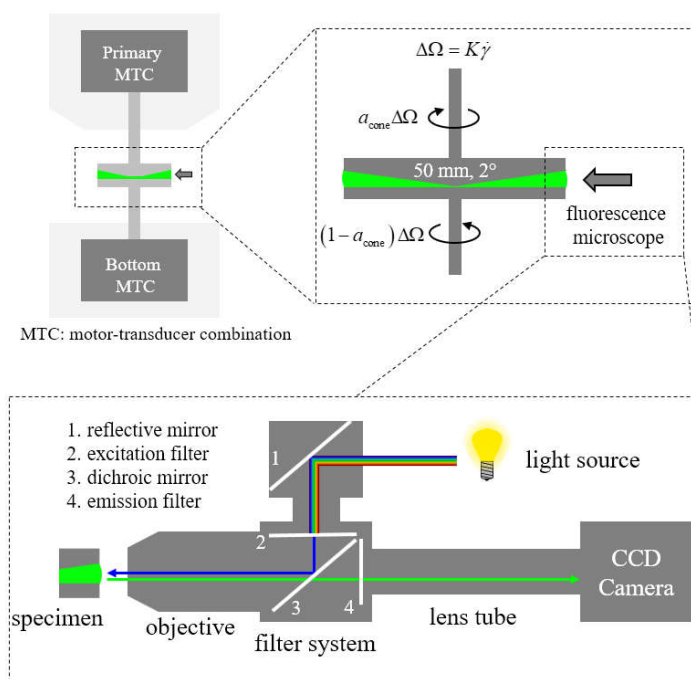


Fig. S1. Schematic of the rheo-PIV instrument.

The MCR 702 rheometer allows the cone and plate to rotate simultaneously at opposite directions with rotational speeds of respectively  $a_{\text{cone}}\Delta\Omega$  and  $(1 - a_{\text{cone}})\Delta\Omega$ . Here,  $a_{\text{cone}}$  is the speed balance coefficient; when  $a_{\text{cone}} = 1$ , only the cone is rotating and when  $a_{\text{cone}} = 0$ , only the plate is rotating.  $\Delta\Omega$  is the rotational speed difference;  $\Delta\Omega$  is proportional to the apparent shear rate  $\dot{\gamma}_0$  which is defined by the

test procedure. We set  $a_{\text{cone}} = 0$  in all the experiments presented in the main manuscript. Some experiments presented in the supplementary materials use different values of  $a_{\text{cone}}$ .

## 2. Supplementary data for PIV algorithm

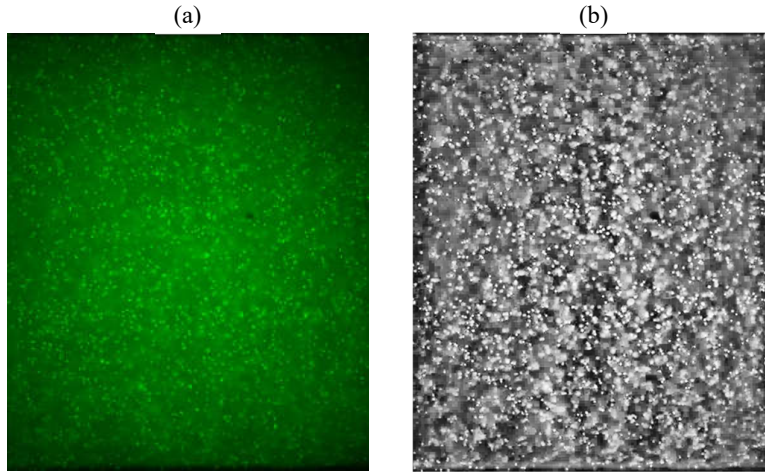


Fig. S2. Effects of contrast-limited adaptive histogram equalization (CLAHE): an image of the field of view (a) before and (b) after CLAHE.

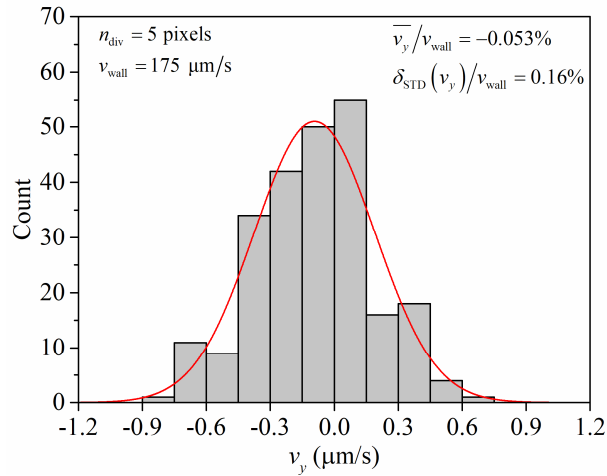


Fig. S3. Histogram of the velocity in the gradient direction ( $v_y$ ) in a Newtonian control fluid under shear at an apparent shear rate of  $0.2 \text{ s}^{-1}$ . This control fluid is a blend of paraffin oil (69 wt%) and polybutene oligomer (31 wt%), seeded with the same tracer particles at the same concentration as used in the fumed silica suspension. Red line is the fit of normal distribution. The wall velocity ( $v_{\text{wall}}$ ) is  $175 \text{ } \mu\text{m/s}$ . The mean ( $\overline{v_y}$ ) and standard deviation ( $\delta_{\text{STD}}$ ) of  $v_y$  are respectively  $-0.053\%$  and  $0.16\%$  of  $v_{\text{wall}}$ .

## 3. Oscillation of shear bands triggered by geometry misalignment

In this section, we show that the cone-and-plate geometry used in this study has slight misalignment which cause oscillation of velocity profiles. Velocimetry oscillation in the fumed silica suspension slowly grows with time and eventually results in noticeable periodical fluctuation of velocity profiles. Velocimetry oscillation in the Newtonian control fluid stays negligible.

Through microscopy, we confirm that the misalignment is within the specifications of the rheometer. Such misalignment is caused by normal manufacturing error and has small impact on Newtonian fluids but can lead to large oscillation of velocity profiles in the thixotropic fumed silica suspension. We find that in the banded flow of the fumed silica suspension, velocity profiles do not remain uniform along the flow direction, and such heterogeneity travels along the flow direction periodically, driven by the rotating geometry. Measurement of velocity profiles, however, relies on the images taken through a microscope at a fixed position. Velocimetry oscillation therefore occurs as the geometry rotates. It is important to understand how the two-dimensional shear bands form and evolve. But it is beyond the scope of this work to make such effort. The rest of this section documents our preliminary findings and analyses.

Note that the fumed silica suspension used in this section (SI-Sec. 3) was made following a slightly different procedure – the last homogenization step prior to rheo-PIV measurements was not performed. Please refer to the third paragraph in the Section of Materials and Instruments in the main manuscript for details about the preparation procedure. This paragraph is copied in Table S1. Omission of the last homogenization step leads to inconsistency in the rheological response (see the discussion on Fig. S7-

e). It may also be what leads to the growth of velocimetry oscillation. But we do not have data either to support or reject this hypothesis. Below we document our characterization of the geometry misalignment and preliminary findings about the velocimetry oscillation in the fumed silica suspension.

Table S1. A paragraph about sample preparation procedure copied from the main manuscript.

“To measure local velocity profiles, we seed fluorescent particles (0.1 vol%, radius = 1.5  $\mu\text{m}$ , Fluoresbrite-YG, Polysciences) into this suspension. The fluid is homogenized using a Cole-Palmer ultrasonic processor (5 min, 500W, 20 kHz) and then put on a bottle roller (9 rpm, Thermo Scientific) for ten days. Before measurement, the suspension is homogenized again through the Cole-Palmer ultrasonic processor (1 min, 500W, 20 kHz) and then is centrifuged at 500 g for 10 seconds to remove air bubbles. The second homogenization prior to rheological tests is important and skipping this step leads to noticeable differences in the rheological response of this suspension, as shown in the supplementary materials.”

We use a simple fluid as a control fluid to determine the extent of geometry misalignment. This control fluid is a blend of paraffin oil (69 wt%) and polybutene oligomer (31 wt%), and it is a Newtonian fluid. We seed fluorescent particles to this fluid to the same concentration as used in the fumed silica suspension. Fig. S4 shows the velocity profiles in this Newtonian fluid under a constant shear rate of  $0.2 \text{ s}^{-1}$ . The velocity profiles undergo slight oscillation as the geometry rotates, which indicates a small amount of geometry misalignment. To gain more detailed information about the geometry misalignment, we track the variation of the wall positions through microscopy as the cone and the plate rotate. Fig. S5 shows that the geometry wall positions fluctuate periodically as the geometry rotates, which indicates misalignment between the spindle and the axis of the geometry. Fig. S6 gives an exaggerated illustration of the geometry misalignment. The geometry tilt angles are calculated based on the data in Fig. S5, and they are smaller than the normal manufacturing error.

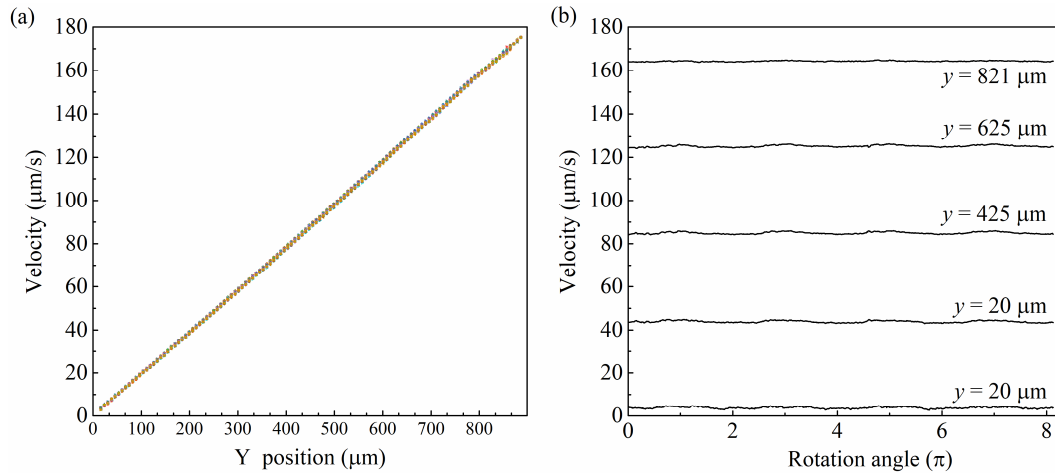


Fig. S4. Velocity profiles in a Newtonian control fluid under constant shear-rate flow ( $\dot{\gamma} = 0.2 \text{ s}^{-1}$ ,  $a_{\text{cone}} = 0$ ). (a) 30 velocity profiles equally spaced in time as the bottom plate rotates for one cycle. (b) Velocity fluctuation at five different  $y$  position across the gap.  $\phi_v$  oscillates between 0.005 and 0.02 in this experiment.

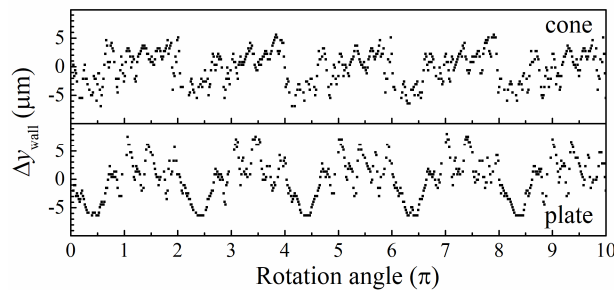


Fig. S5. Variation of the positions of the geometry walls as both the cone and the plate rotate at a constant speed of 0.035 rad/s. Wall positions are determined through microscopy.

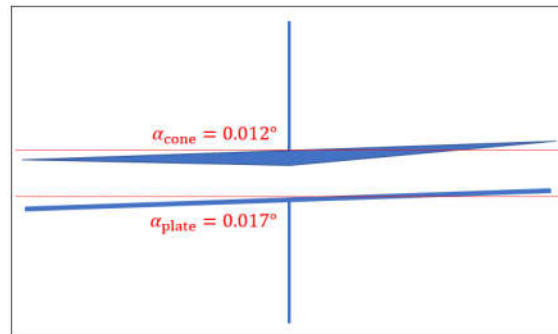


Fig. S6. Exaggerated illustration of the geometry misalignment. Normal manufacturing error is 0.02 degrees for both the cone and the plate geometries.

In contrast to the small oscillation of velocity profiles in the Newtonian fluid ( $\phi_v$  oscillates between 0.005 and 0.02), the banded flow of the thixotropic suspension exhibits much larger oscillations. Fig. S7 shows the evolution of the stress and  $\phi_v$  in

a group of constant-shear-rate experiments with  $\dot{\gamma}_0 = 0.075 \text{ s}^{-1}$  and  $a_{\text{cone}} = 1, 0.75, 0.5, 0.25,$  and  $0$ . The duration of the experiments are at least 7 hours. The strain imposed on the sample exceeds 1890 strain units, which is much larger than that in shear start-up and flow reversal experiments. Note that as  $a_{\text{cone}}$  changes, the period of rotation of the geometry changes, following the relationships  $t_{\text{cone}} \propto 1/a_{\text{cone}}$  and  $t_{\text{plate}} \propto 1/(1 - a_{\text{cone}})$ .

$\phi_v(t)$  exhibits periodic oscillations in all five experiments. The amplitude of the oscillation and the exact values of  $\phi_v(t)$  vary significantly in the five experiments. Although the long-term banding dynamics lacks reproducibility, the periodicity displays a distinct dependence on the rotation of the geometry. The periodicity can be determined through discrete Fourier transforms (inserts in Fig. S7) of  $\phi_v(t)$ . The results show that  $\phi_v(t)$  displays a period equal to either the rotation period of the plate or of the cone,  $t_{\text{plate}}$  or  $t_{\text{cone}}$ , whichever is smaller.  $\phi_v(t)$  may simultaneously exhibit a faster oscillation in addition to the one set directly by the rotation of the geometry.

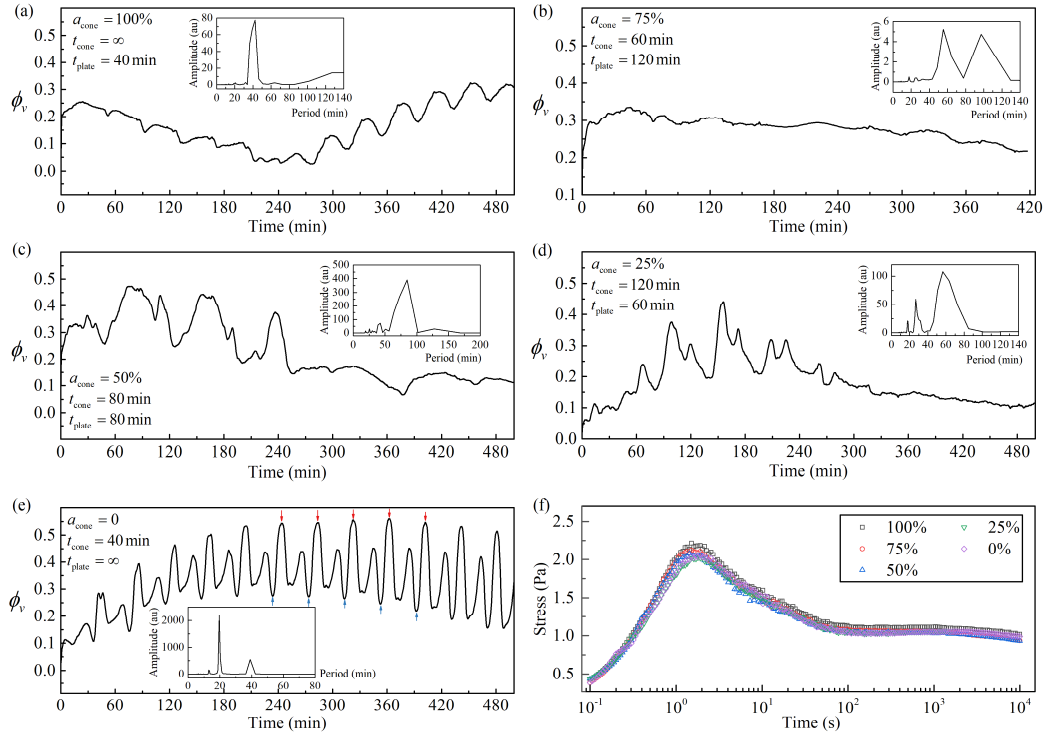


Fig. S7. (a-e) Oscillation of shear bands under a constant apparent shear rate of  $0.075 \text{ s}^{-1}$  while varying  $a_{\text{cone}}$ . Corresponding rotation periods of the cone and plate,  $t_{\text{cone}}$  and  $t_{\text{plate}}$  are given in annotations. Inserts show the coefficients of the discrete Fourier transforms of  $\phi_v$ . The velocity profiles at the times marked by the colored arrows in (e) are given in Fig. S8. (f) Rheological response in the five experiments of (a-e).

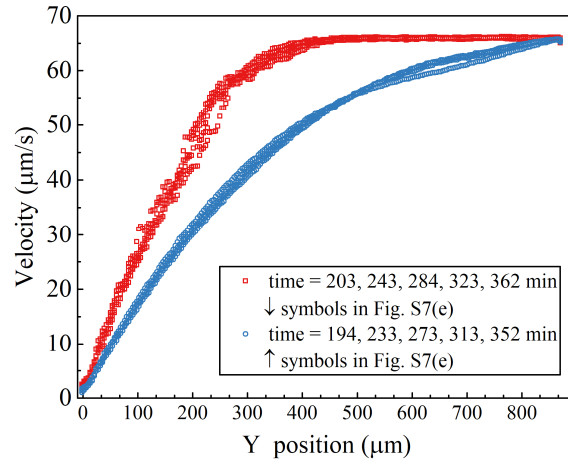


Fig. S8. Velocity profiles at selected time points in Fig. S7(e).

The velocity profiles at several time points as indicated in Fig. S7(e) are given in Fig. S8. When  $\phi_v$  takes peak values, a plug flow forms that occupies around 50% of

the geometry gap. The plug flow vanishes and recurs as the geometry rotates, which results in the large periodic oscillation of  $\phi_v$  as shown in Fig. S6(e).

Although the long-term banding dynamics exhibits noticeable oscillation and lacks reproducibility in the series of experiments of Fig. S7, the bulk rheological responses are very similar in the five experiments and show no sign of oscillation.

The stress responses presented in Fig. S7(e) are inconsistent with those in Fig. 5(a). The inconsistency can be seen from two aspects: 1) the stress responses in Fig. S7(e) do not clearly show a second overshoot or kink while the stress responses in Fig. 5(a) show this signature; 2) the stress response in Fig. S7(e) approaches to a plateau at around 1 Pa while those in Fig. 5(a) (judging from the data of the two tests with  $\dot{\gamma}_0 = 0.05$  and  $0.1 \text{ s}^{-1}$ ) seemingly approaches to a plateau at around 2 Pa.

The velocimetry oscillation driven by geometry rotation suggest the possibility of flow heterogeneity along the flow direction. A traveling wave presumably forms as the shear bands carried by the rotating geometry cross through the velocimetry observation window. To test this hypothesis, we reprocess the video for PIV analysis from the experiment of Fig. S7 (e) and calculate separately the velocity profiles in the left-most region and the right-most region of the field of view (FOV) (as illustrated in Fig. S9). We then compare the difference in velocity profiles in the two regions. Note that we use a large FOV (2.6 mm  $\times$  0.87 mm) in this experiment to better resolve the velocity difference along the flow direction. In this experiment,  $a_{\text{cone}} = 0$ , and therefore  $v_{\text{cone}} = 0$ ,  $v_{\text{plate}} = 0.0655 \text{ mm/s}$ . The distance between the two regions is 2.2 mm.

It takes around 34 seconds for a tracer particle sticking to the rotating plate to travel from the left-most region to the right-most region.

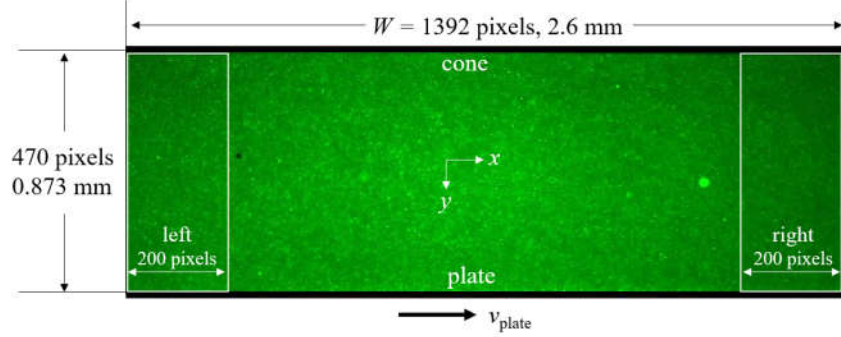


Fig. S9. A sample image of the field of view for PIV calculation in the test of Fig. S7 (e).

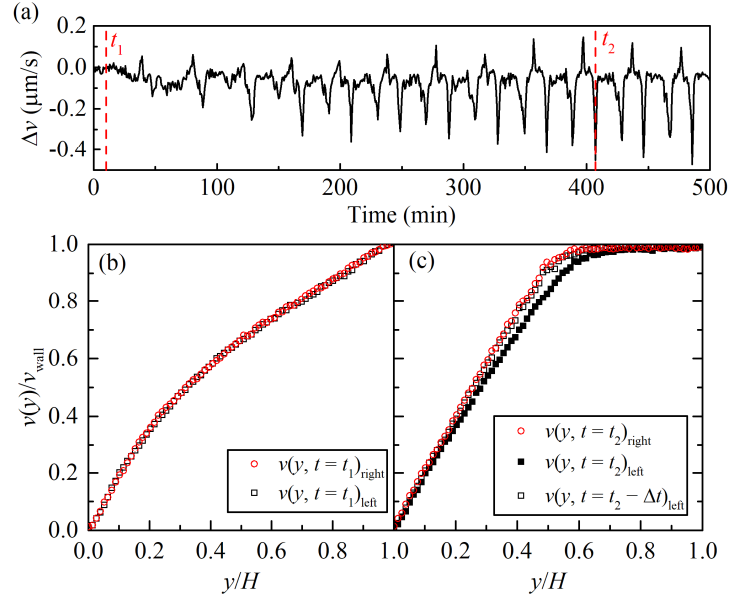


Fig. S10 Evidence of traveling shear bands. Results are from the test of Fig. S7 (e). (a) The evolution of  $\Delta v$ . (b)  $v_{\text{left}}(y, t_1)$  and  $v_{\text{right}}(y, t_1)$  with  $t_1 = 10$  min. (c)  $v_{\text{left}}(y, t_2)$ ,  $v_{\text{left}}(y, t_2 - \Delta t)$ , and  $v_{\text{right}}(y, t_2)$  with  $t_2 = 410$  min and  $\Delta t = 34$  s.

Fig. S10 (a) shows the evolution of  $\Delta v$  which is defined as

$$\Delta v = v_{\text{left}}(y = H/2, t) - v_{\text{right}}(y = H/2, t) \quad (\text{S1})$$

where  $v_{\text{left}}(y, t)$  and  $v_{\text{right}}(y, t)$  are the velocity profiles in respectively the left-most region and the right-most region of the FOV.  $\Delta v$  provides a measure of the velocity heterogeneity along the flow direction in the fluid layer of  $y = H/2$ . Fig. S10 (a) shows that  $\Delta v$  is small during the first 30 minutes after the shear start-up. An

oscillation of  $\Delta v$  then occurs and gradually amplifies. The two regions have very similar velocity profiles during the first 30 mins. Fig. S10 (b) shows the velocity profiles at  $t = t_1 = 10$  min. As the oscillation of  $\Delta v$  amplifies, the difference between  $v_{\text{left}}(y, t)$  and  $v_{\text{right}}(y, t)$  increases. For example, at  $t = t_2 = 410$  min,  $v_{\text{left}}(y, t_2)$  and  $v_{\text{right}}(y, t_2)$  exhibit a noticeable difference. Interestingly,  $v_{\text{left}}(y, t_2 - \Delta t)$  and  $v_{\text{right}}(y, t_2)$  have very similar values when  $\Delta t = 34$  s, the time it takes for a shear band moving at a velocity of  $v_{\text{wall}}$  to cross through the two PIV regions. With the results shown in Fig. S10, we confirm that during the long period of shearing, the flow forms bands with heterogeneity in both the flow direction and the gradient direction, and velocimetry oscillation occurs as the bands travel through the PIV windows periodically following the rotation of the geometry.

#### 4. Two-dimensional velocity profiles

In this section, we confirm through 2D PIV algorithm<sup>1</sup> that the flow field in the fumed silica suspension is close to 1D shear flow, i.e.,  $v_y \approx 0$  across the flow cell. For simplicity, we provide two examples. Fig. S11 shows  $v_y(x)$  which is the average value of  $v_y(x, y)$  across  $y$  at several time points over the test.  $v_y(x)$  remains insignificant (lower than 1% of  $v_{\text{wall}}$ ) over the experiment.

---

<sup>1</sup> William Thielicke (2019). PIVlab - particle image velocimetry (PIV) tool (<https://www.mathworks.com/matlabcentral/fileexchange/27659-pivlab-particle-image-velocimetry-piv-tool>), MATLAB Central File Exchange. Retrieved August 28, 2019.

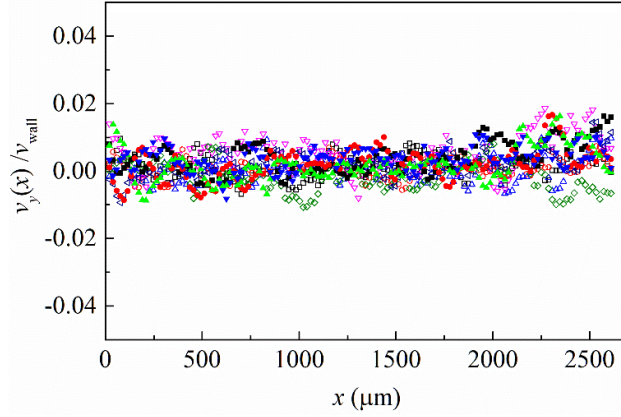


Fig. S11 1D velocity (y-component) profile  $v_y(x)$  in the experiment of Fig. S7(e) at  $t = 1.5, 4.4, 1.3 \times 10^1, 3.9 \times 10^1, 1.2 \times 10^2, 3.6 \times 10^2, 1.1 \times 10^3, 3.2 \times 10^3, 9.6 \times 10^3, 2.9 \times 10^4$  s.  $v_{\text{wall}}$  is the velocity of the moving wall.

Fig. S12 shows the 2D velocity profile in the shear startup test ( $\dot{\gamma}_0 = 0.01 \text{ s}^{-1}$ ) of the fumed silica suspension at several strain values, and Fig. S13 shows the corresponding profile of  $v_y(x)$ . Fig. S12 and Fig. 13 show that  $v_y \approx 0$  in this experiment.

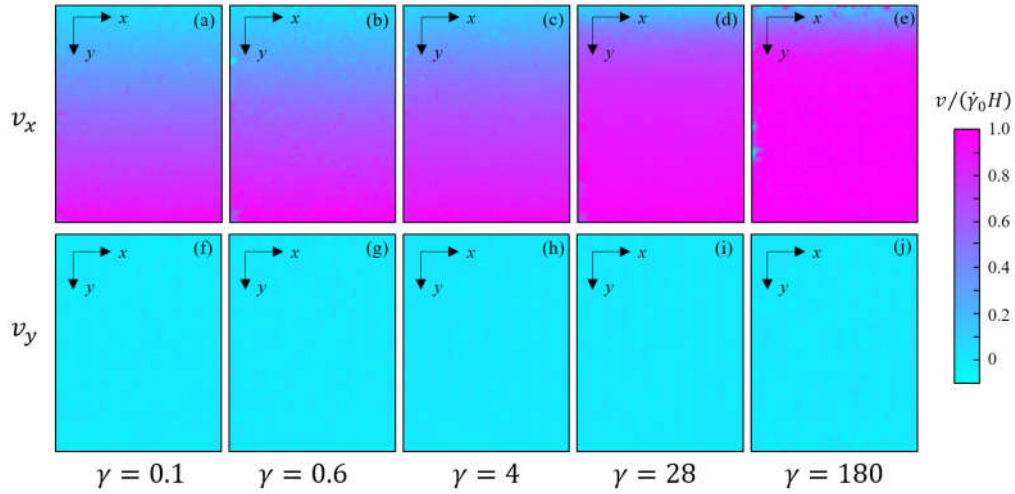


Fig. S12 Two-dimensional spatial distribution of (a-e) the x component and (f-j) the y component of the velocity in the shear startup test ( $\dot{\gamma}_0 = 0.01 \text{ s}^{-1}$ ) of the fumed silica suspension. Background color reflects the value of velocity normalized by  $\dot{\gamma}_0 H$  as indicated by the color bar. The corresponding strain units are 0.1 in (a, f), 0.6 in (b, g), 4 in (c, h), 28 in (d, i), and 180 in (e, j). The boundary of each panel indicates the boundary of the field of view for 2D-PIV analysis: upper boundary, wall of the cone; lower boundary, wall of the bottom plate. The flow remains nearly one-dimensional

because  $v_y \approx 0$  through the test as shown by the uniform color corresponding to zero velocity in the bottom images.

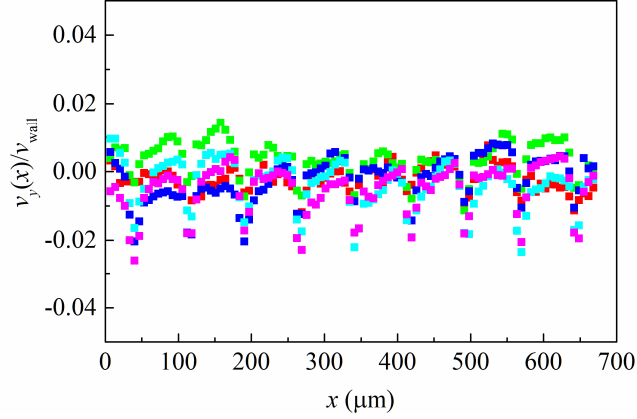


Fig. S13 1D velocity (y-component) profile  $v_y(x)$  the shear startup test ( $\dot{\gamma}_0 = 0.01 \text{ s}^{-1}$ ) of the fumed silica suspension at  $\gamma = 0.1, 0.6, 4, 28, 180..$

## 5. Dynamics of local flow heterogeneities

The local shear rate heterogeneity in experimental shear startup tests is  $\delta\dot{\gamma}(y)$  which is defined by Eq. (S2), the same as Eq. (5) in the main manuscript.

$$\delta\dot{\gamma}(y,t) = \dot{\gamma}(y,t) - \dot{\gamma}_0. \quad (\text{S2})$$

For a given velocity profile, we calculate the local shear rate by dividing each velocity profile into ten adjacent regions equally spaced across the gap and fitting each sub-region with a linear function. Fig. S14 is based on the data from the shear startup test of  $\dot{\gamma}_0 = 0.01 \text{ s}^{-1}$ . The figure shows that  $\delta\dot{\gamma}$  at different  $y$  positions can roughly fall onto a master curve if rescaled with appropriate factors.

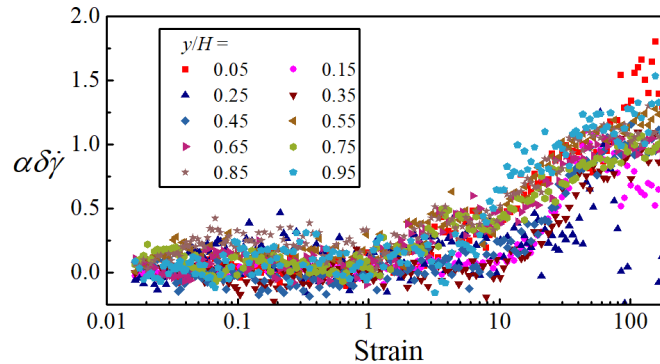


Fig. S14 Evolution of the local shear rate heterogeneities,  $\delta\dot{\gamma}(y) = \dot{\gamma}(y) - \dot{\gamma}_0$ , in ten adjacent equal-width sub-regions of the velocity profiles. In  $\alpha$  is the rescaling factor which is constant for each sub-region, with values of 0.03287, 0.02153, 0.0069, -0.00863, -0.00863, -0.00863, -0.00863, -0.00863, -0.00863, and -0.00863 for the ten sets of data as  $y/H$  increases.

## 6. Oscillatory shear test

### 6.1 Strain amplitude sweep

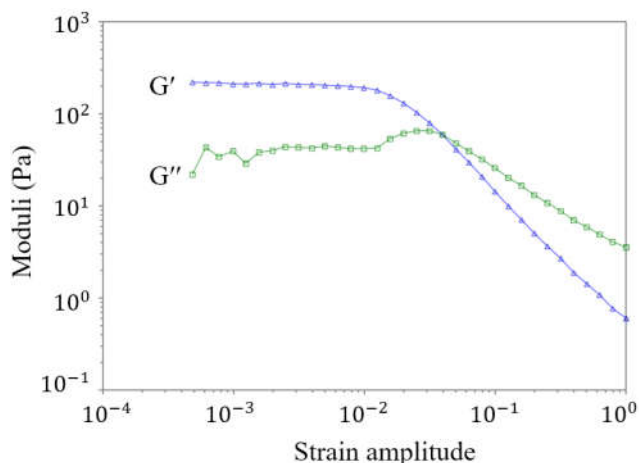


Fig. S15. Rheological response of the fumed silica suspension in an oscillatory amplitude sweep test.  $G'$ , elastic modulus;  $G''$ , loss modulus. Oscillatory frequency is 1 rad/s. The crossover point where  $G' = G''$  occurs at a strain amplitude of around 0.04. The sample was pre-sheared at  $200 \text{ s}^{-1}$  for 2 minutes and then rested for 2 hours prior to this test.

### 6.2 Oscillatory frequency sweep

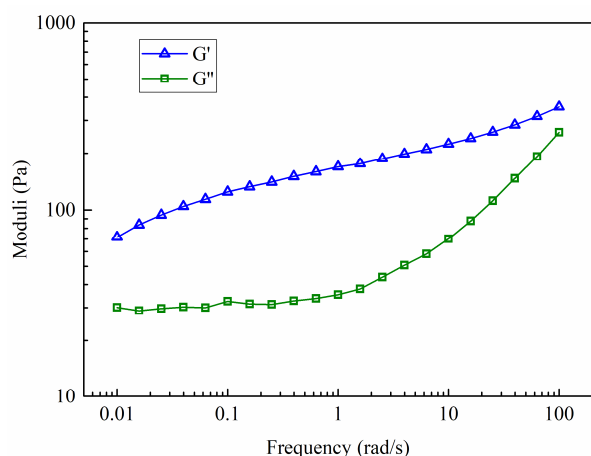


Fig. S16. Rheological response of the fumed silica suspension in an oscillatory frequency sweep test.  $G'$ , elastic modulus;  $G''$ , loss modulus. Oscillatory strain is 1%. The sample was pre-sheared at  $200 \text{ s}^{-1}$  for 2 minutes and then rested for 2 hours prior to this test.

### 6.3. Growth of moduli after cessation of shearing

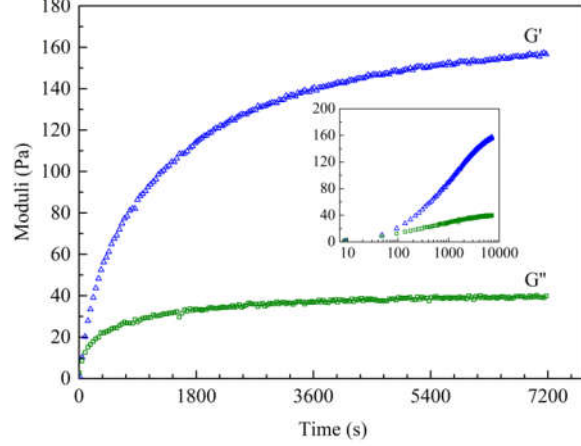


Fig. S17. Growth of the elastic and loss moduli of the fumed silica suspension after a pre-shear at  $200 \text{ s}^{-1}$  for 2 minutes. Oscillatory frequency, 1 rad/s; oscillatory strain, 1%. Insert shows the same data with logarithmic scale of time.

## 7. Model parameterization

At steady state, considering only positive shear rates, the model predicts a flow curve that follows Eq. (S3):

$$\sigma_{\text{ss}}(\dot{\gamma}) = \frac{C}{q + k_A/\dot{\gamma}} + \frac{\sigma_{y0}}{K\dot{\gamma}/k_\lambda + 1} + \left( \frac{\eta_{\text{thi}}}{K\dot{\gamma}/k_\lambda + 1} + \eta_n \right) \dot{\gamma}, \quad (\text{S3})$$

which contains 8 parameters, which is all of the parameters, except for the stress diffusivity  $D$ . The apparent viscosity at the high-shear-rate limit is  $\lim_{\dot{\gamma} \rightarrow \infty} \sigma_{\text{ss}}/\dot{\gamma} = \eta_n$ , which can be determined from the experimental flow curve. As the shear rate approaches zero, the stress approaches a plateau,  $\lim_{\dot{\gamma} \rightarrow 0} \sigma_{\text{ss}} = \sigma_{y0}$ . This plateau, however, is difficult to directly estimate because it lies in the region  $\dot{\gamma} < 10^{-5} \text{ s}^{-1}$  which is not practical to measure.

Note that in Eq. (S3)  $k_A$  is the characteristic restructuring rate coefficient of the back strain  $A$ , and  $k_\lambda$  is the growth rate of the thixotropic structure parameter  $\lambda$ . In his model,  $A$  is thought to capture the level of anisotropy in the internal structures and  $\lambda$  to capture the overall degree of aggregation of the internal structures. From flow

reversal tests and thixotropic buildup tests, we confirm that  $k_A$  and  $k_\lambda$  are both much smaller than  $1 \text{ s}^{-1}$ .

At very small strain rate, the middle term of Eq. (S3) dominates and produces a constant stress equal to the yield value  $\sigma_{y0}$ . As the shear rate rises to around  $\dot{\gamma} \approx k_A$ , the first term on the right side of Eq. (S3) becomes significant, which gives a positive slope to the flow curve. The flow curve thus rises from the yield stress to reach a second plateau in the region where  $\dot{\gamma} \approx k_A$ ,  $\sigma_{ss}(0 < \dot{\gamma} \approx k_A \ll 1 \text{ s}^{-1}) \approx \frac{c}{q+1} + \sigma_{y0}$ . As a result, one can get an estimation of the values of  $k_A$  and  $\frac{c}{q+1} + \sigma_y$  from the experimental flow curve. The parameter  $q$  dominates the characteristic strain scale in flow reversal tests. We found that  $q = 1$  agrees with experiments well.

To estimate the values of the other free parameters, one needs to fit the model to some experimental data, including the flow curve, a flow reversal test, and a thixotropic buildup test (in which  $\dot{\gamma}$  instantly jumps from a large value to a small one).

## 8. Model parameterization

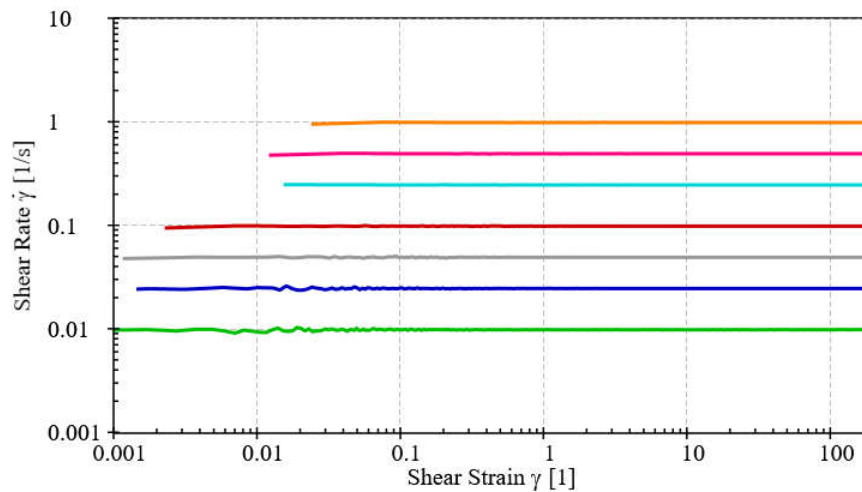


Fig. S18. Actual apparent shear rate imposed by the rheometer in the set of experiments of Fig. 5

### 9. Apparent flow curve of heterogeneous flow

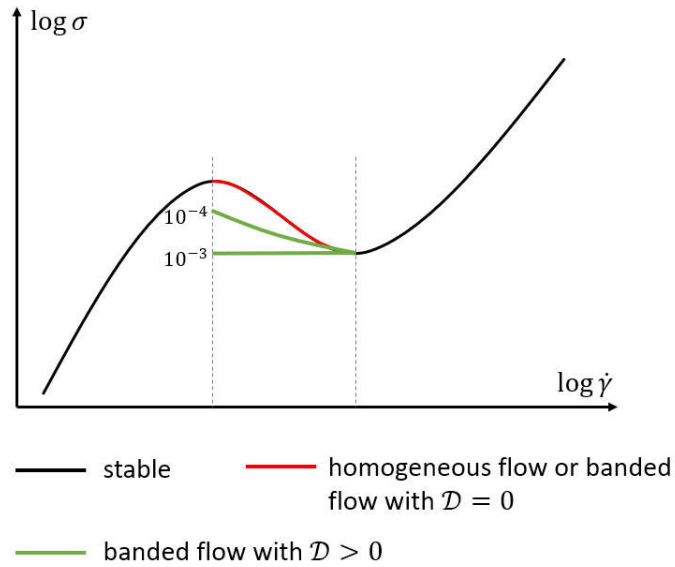


Fig. S19 Illustration of the effects of the value of  $\mathcal{D}$  on the apparent flow curve of the banded flow.  $\mathcal{D} = D/H^2$  where  $D$  is the diffusion coefficient in the model and  $H$  is the gap.

### 10. Supplementary data for Fig. 9 and Fig. 5.

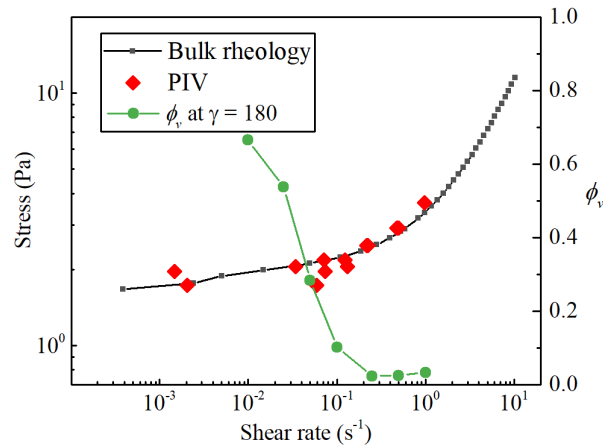


Fig. S20 Pseudo-steady flow curve determined from the bulk rheometry and local velocimetry, and the value of  $\phi_v$  at  $\gamma = 180$  in the set of shear startup tests of Fig. 5(a).